Intrinsic Distribution and Atomic Level Stress in Polymeric Melts

R. C. Picu

Department of Mechanical Engineering, Aeronautical Engineering and Mechanics, Rensselaer Polytechnic Institute, Troy, New York 12180

Received May 27, 1999; Revised Manuscript Received July 26, 1999

ABSTRACT: The relationship between stress production and relaxation on one hand and the local structure on the other is studied in model polymeric melts by the use of equilibrium and nonequilibrium molecular dynamics. The analysis is performed in the intrinsic coordinate system—a mobile frame tied to the generic bond. The variation of the intrinsic distribution of interacting neighbors about a representative atom, $\tilde{g}$, with density and temperature is investigated above and below the glass transition. It is shown that $\tilde{g}$ captures close packing effects and the buildup of structure upon transition, similar to the radial distribution function $g(\mathbf{r})$. When computed from the nearest nonbonded neighbors, the intrinsic distribution is nonuniform due to steric shielding. Neighbors at distances larger than a covalent bond length from the representative atom, however, lead to a uniform distribution $\tilde{g}$. Thus, the steric shielding effect generates a nonzero intrinsic deviatoric stress in both equilibrium and nonequilibrium systems, while longer range interactions do not contribute to deviatoric stress production. Consequently, each intrinsic frame carries a nonhydrostatic stress (induced by both bonded and nonbonded interactions) which, upon rotation in the global coordinate system, contributes to the global stress in the melt. A preferential orientation of intrinsic frames (induced, for instance, by the deformation of the fluid) generates therefore a deviatoric global stress. In nonequilibrium simulations, the intrinsic distribution is seen to be independent of the deformation of the fluid. Furthermore, when computed from chain inner atoms, the intrinsic distribution is also chain length independent. This implies, in turn, that intrinsic stresses are deformation and chain length independent. The relevance of these observations to stress relaxation in polymeric melts is discussed.

1. Introduction

The deformation of a polymeric melt induces atomic-level structural changes that ultimately account for stress production. Such effects have been evidenced by the use of atomistic simulations in a number of works,[1−5] and in systems of various degrees of complexity. Recently, the correlation between the deformation of the neighborhood of a representative atom and stress has been made quantitative for idealized melt models of the "pearl-necklace" type.[4,5] This work established the relationship between the regimes of stress relaxation and structural changes. It is the purpose of the present investigation that of introducing a structural invariant to melt deformation and of establishing its role in stress production and relaxation.

Most treatments of viscoelasticity in polymeric systems are on the molecular level,[6−8] with chains regarded as entropic springs in tension. The macroscopic deviatoric stress arising during melt deformation is assumed to be due to chain stretching which reflects in a change in the entropy and free energy of the system. In this molecular description, deviatoric stress is produced by bonded interactions, while interactions between nonbonded atoms are assumed to give rise only to a hydrostatic stress.

The inability of the molecular picture of stress production to account for a number of effects such as the behavior of small molecular systems and the high-frequency response,[9,10] stimulated the development of an atomic-level description.[11−15] In this new framework, stress is computed on the atomic level by explicitly considering both bonded and nonbonded interactions. Moreover, it was shown that the contribution to stress of nonbonded interactions is more significant than that of bonded interactions. These effects have been quantified by decomposing the total stress in three components[13] and by the use of the intrinsic stress concept.[16] The intrinsic stress is the stress associated with an atom and projected in a coordinate system tied to the respective bond of the chain. The intrinsic frame is therefore mobile and the macroscopic stress is given by the sum of "stresslets" (intrinsic stress tensors) rotated in the global coordinate system. Interestingly, it was observed that the intrinsic stress tensor is insensitive to the deformation of the melt and is therefore a system parameter for given thermodynamic conditions. Furthermore, the stress−optical coefficient representing the ratio of birefringence to global stress, can be expressed in terms of intrinsic stresses.[5,15] These remarkable properties point to the investigation of the structural origins of the intrinsic stress. The results of this investigation are discussed next.

The outline of the paper is as follows: A description of the model and the algorithm employed are presented in section 2; the concept of intrinsic stress is reviewed in section 3, while in section 4 the relevance of the intrinsic distributions to intrinsic and global deviatoric stress production and relaxation is discussed. The conclusions are summarized in section 5.

2. Model Description and Simulation Procedure

The principal tool in this investigation is the computer simulation of model systems consisting of dense collections of molecules. The molecules are represented by a "pearl necklace" type model in which particles represent atoms linked into chains by stiff linear springs simulating covalent bonds. Short molecules of four atoms per chain ($N_b = 3$; N_b stands for the number of bonds per chain) as well as long chains ($N_b = 200$) are considered. The covalent bond between the pair of atoms of each

10.1021/ma990836q CCC: $18.00
Published on Web 09/25/1999

molecule is represented by the potential

$$u_b(r) = \frac{1}{2}\kappa(r - b)^2 \tag{1}$$

and all nonbonded atoms interact with a truncated Lennard−Jones potential

$$u_{nb}(r) = \begin{cases} 4\epsilon_{LJ}\left(\left(\frac{\sigma_{LJ}}{r}\right)^{12} - \left(\frac{\sigma_{LJ}}{r}\right)^{6}\right) & r \le R_c \\ u_{nb}(R_c) & r > R_c \end{cases} \tag{2}$$

where r denotes the distance between any pair of atoms and b is the bond length. The spring constant κ has a value corresponding to $\kappa b^2/k_B T = 267$ and $b = \sigma_{LJ}$. In the present simulations, $R_c = 2^{1/6}\sigma_{LJ}$ so that only the repulsive part of the potential is considered. The units of length, energy and time of the problem are respectively σ_{LJ}, ϵ_{LJ}, and $\sigma_{LJ}\sqrt{m_0/\epsilon_{LJ}}$, where m_0 is the atomic mass. The units employed for stress are $\epsilon_{LJ}/\sigma_{LJ}^3$.

Periodic boundary conditions are used in the simulations as customary in molecular dynamics. The basic cell referred to a Cartesian system is, in the equilibrium state, a cube of dimensions L. There are N atoms per unit cell, which leads to a reduced density

$$\rho = \frac{N\sigma_{LJ}^3}{L^3} \tag{3}$$

The simulation begins with the atoms being arranged in an fcc pattern and with a random velocity field. A high-temperature equilibration is performed to obtain a proper melt structure. In simulations of short chain molecules ($N_b = 3$), the system was composed from $N = 632$ atoms, while long chain systems ($N_b = 200$) contained $N = 4025$ atoms.

The algorithm used to integrate the equations of motion as well as the thermostat are those due to Berendsen et al.[17] The position of a particle at time $(t + \Delta t)$ is obtained from its position at time t and that at $(t - \Delta t)$ by

$$\mathbf{x}(t + \Delta t) = (1 + \xi)\mathbf{x}(t) - \xi\mathbf{x}(t - \Delta t) + \xi\frac{\mathbf{f}}{m_0}\Delta t \tag{4}$$

where the force $\mathbf{f}$ acting on the atom in question is determined from the atomic positions at time t. The scaling factor ξ is given by the equation

$$\xi = \left[1 + \frac{\Delta t}{\Omega}\left(\frac{T_o}{T(t - \Delta t/2)} - 1\right)\right]^{1/2} \tag{5}$$

where T_o is the target temperature and $T(t - \Delta t/2)$ is calculated based on the velocities at time $(t - \Delta t/2)$ obtained from

$$\mathbf{v}(t - \Delta t/2) = \frac{\mathbf{x}(t) - \mathbf{x}(t - \Delta t)}{\Delta t} \tag{6}$$

The parameter Ω controls the speed of response of the algorithm to a perturbation in temperature. For our simulations performed under high strain rate−high energy input conditions, this parameter is taken as $\Omega = 10\ \Delta t$. For this value, it was verified that the temperature at the onset of relaxation is the target temperature and remains so through the remaining relaxation. The time step of integration Δt is kept constant for the whole loading−relaxation history and is equal to 0.001. It was verified that a further decrease in Δt did not affect the results.

Simulations are performed under both equilibrium and nonequilibrium conditions. In nonequilibrium runs, the deformation of the melt is induced by a volume-preserving elongational deformation of the unit cell. During such a deformation, with the stretch direction x_1, the cell size is modified according to

$$\begin{aligned} L_1 &= L(1 + \dot\epsilon t) \\ L_2 &= L/(1 + \dot\epsilon t)^{1/2} \\ L_3 &= L/(1 + \dot\epsilon t)^{1/2} \end{aligned} \tag{7}$$

where $\dot\epsilon$ is the deformation strain rate. All simulations reported here are performed with a strain rate $\dot\epsilon = 0.1$, and the total deformation of the cell in the stretch direction is 10%. The periodic boundary conditions remain unchanged during deformation.

To reduce the noise in the measured quantities, the calculation has to be repeated N_c number of times using independent initial conditions and the results are averaged over all runs. The results reported here are obtained by averaging over $N_c = 200$ simulations for the short chain system and over $N_c = 12$ simulations for the $N_b = 200$ case.

3. Intrinsic Stresses

The stress t_{ij} in the melt expressed in the global coordinate system of the simulation cell is computed using the virial stress formula[18]

$$vt_{ij} = -NkT\delta_{ij} + \frac{1}{2}\sum_{m=1}^{N}\left\langle \sum_{n=1}^{N_m} r_{mn}^{-1}u'_{mn}(r_{mn})r_{mni}r_{mnj}\right\rangle \tag{8}$$

where $v = L^3$ is the volume of the unit cell and r_{mn} is the length of the vector $\mathbf{r}_{mn}$ between interacting atoms m and n and has components r_{mni}, and $u' = du/dr$. The first sum is taken over all atoms in the system while the second is over all N_m atoms interacting with atom m at time t and in a given simulation. The contribution to stress of both bonded and nonbonded interactions is considered, with u_{mn} representing the respective potential. The kinetic contribution $-NkT$ is assumed to affect the hydrostatic stress only since the thermal velocities are much higher than those due to deformation (in nonequilibrium). The angular bracket represents averaging over all N_c simulations.

The nonkinetic contribution to global stress of a representative atom m, at time t and in a given simulation, is therefore

$$\sigma_{ij}^{m} = \frac{1}{2v}\sum_{n=1}^{N_m} r_{mn}^{-1}u'_{mn}(r_{mn})r_{mni}r_{mnj} \tag{9}$$

with the total stress of eq 8 becoming

$$t_{ij} = -\rho kT\delta_{ij} + \sum_{m=1}^{N}\langle\sigma_{ij}^{m}\rangle \tag{10}$$

The intrinsic stresses are defined for each atom, in an intrinsic coordinate system $\tilde{x}_r$ as shown in Figure 1. Let $\mathbf{e}_i$ be the unit base vectors of the x_i system tied to the simulation cell, and $\mathbf{a}_r^m$ the corresponding vectors

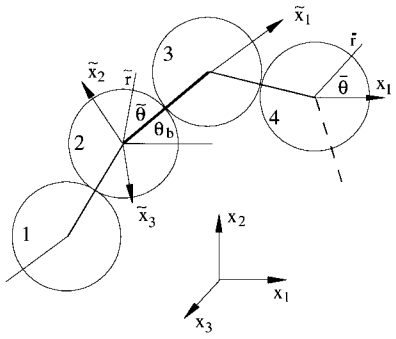

Figure 1. Intrinsic and global coordinate system. The global coordinate system x_i is fixed in the laboratory coordinates. The intrinsic coordinate system for atom 2 is shown, with $\tilde{x}_1$ taken by definition along the covalent bond between atoms 2 and 3.

of the $\tilde{x}_r$ system. The index m shows that the intrinsic coordinate system $\tilde{x}_r$ has a different spatial orientation for each atom (bond) m in the system. The atomic level stress $\sigma_{ij}{}^m$ of eq 9 can be expressed in the intrinsic system $\tilde{x}_r$ as

$$\tilde{\sigma}_{rs}{}^m = \sigma_{ij}{}^m a_{ri}{}^m a_{sj}{}^m \tag{11}$$

where $a_{ri}{}^m = \mathbf{a}_r^m \cdot \mathbf{e}_i$ are components of the rotation matrix relating the global and intrinsic coordinate systems. The intrinsic stress tensor $\langle\langle\tilde{\sigma}_{rs}\rangle\rangle$ is obtained by averaging $\tilde{\sigma}_{rs}{}^m$ over all N atoms in the system and over all N_c simulations.

The intrinsic stress is a cylindrical tensor in which the only nonzero components are $\langle\langle\tilde{\sigma}_{11}\rangle\rangle$ and $\langle\langle\tilde{\sigma}_{22}\rangle\rangle = \langle\langle\tilde{\sigma}_{33}\rangle\rangle$. Most remarkably, it was observed that, when computed from atoms which are not at the chain ends, its components are independent of chain length.[15] Furthermore, the intrinsic stress tensor computed from equilibrium simulations has the same value with that computed from nonequilibrium simulations except for a small variation during the loading period.[15,16] Since the intrinsic stress is directly related to the global stress t_{ij} through eq 10 and 11, its invariance with respect to deformation and chain length suggests that it can be used to great advantage in describing stress production and relaxation.

4. Intrinsic Distributions

The relationship between intrinsic stresses and the atomic structure about a representative atom can be studied in the intrinsic coordinate system $\tilde{x}_r$ (Figure 1) by introducing an intrinsic distribution function $\tilde{g}(\tilde{\mathbf{r}})$. This function, defined in intrinsic coordinates, is similar to the standard radial distribution function $g(\mathbf{r})$ defined in the global coordinate system x_i. In spherical coordinates and in the vicinity of each atom, $\tilde{g}(\tilde{\mathbf{r}}) = \tilde{g}(\tilde{r},\tilde{\theta},\tilde{\varphi})$, where $\tilde{\theta}$ is the angle between $\tilde{\mathbf{r}}$ and $\mathbf{a}_1{}^m$, the unit vector aligned with $\tilde{x}_1$. Because of symmetry, there is no dependence on $\tilde{\varphi}$, and hence $\tilde{g}(\tilde{\mathbf{r}}) = \tilde{g}(\tilde{r},\tilde{\theta})$. Since only interacting neighbors need to be considered, the range of $\tilde{r}$ is limited to $0 < \tilde{r} < R_c$, where R_c is the interaction cutoff distance, eq 2.

For the present purposes, it was found useful to characterize $\tilde{g}(\tilde{\mathbf{r}})$ at any time t by two parameters defined as

$$\tilde{\bar{r}}(\tilde{\theta}) = \frac{\int_0^{R_c} \tilde{r}\tilde{g}(\tilde{r},\tilde{\theta})\tilde{r}^2\,d\tilde{r}}{\int_0^{R_c} \tilde{g}(\tilde{r},\tilde{\theta})\tilde{r}^2\,d\tilde{r}} \tag{12}$$

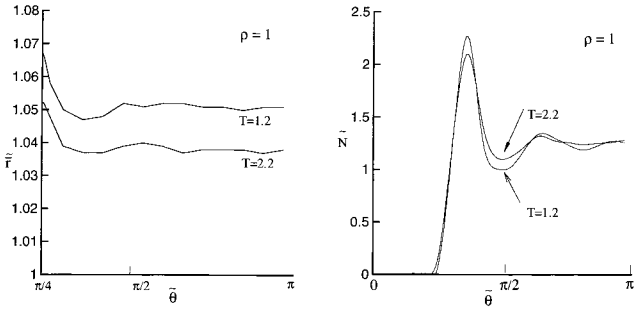

Figure 2. Intrinsic distribution of interacting atoms surrounding a representative atom of the system with density $\rho = 1$ and, in the liquid state, at temperatures $T = 1.2$ and 2.2.

and

$$\tilde{N}(\tilde{\theta}) = \frac{3}{R_c{}^3}\int_0^{R_c} \tilde{g}(\tilde{r},\tilde{\theta})\tilde{r}^2\,d\tilde{r} \tag{13}$$

These parameters are similar to $\bar{r}$ and $\bar{N}$ introduced in ref 4 in order to characterize the radial distribution function in global coordinates.

The parameter $\tilde{\bar{r}}$ represents the mean radius of interacting neighbors, while $\tilde{N}$ represents their number density, both measured at angle $\tilde{\theta}$. As with $\bar{r}$ and $\bar{N}$, $\tilde{\bar{r}}$ describes the "shape" of the neighborhood, while $\tilde{N}$ describes the atom number density distribution. For convenience, $\tilde{N}$ is normalized such that the average intrinsic number density equals the imposed density ρ of the system. The two atoms that are covalently bonded to the representative atom are not taken into account while computing $\tilde{\bar{r}}$ and $\tilde{N}$. Both $\tilde{\bar{r}}$ and $\tilde{N}$ are computed by dividing the neighborhood of the representative atom in sectors of $\Delta\tilde{\theta} = 10°$ span.

The two parameters $\tilde{\bar{r}}$ and $\tilde{N}$ have been computed in equilibrium and following a constant volume deformation, and their dependence on density and temperature as well as their evolution during stress relaxation was determined. These results are discussed next.

Equilibrium Simulations. Figure 2 shows $\tilde{\bar{r}}$ and $\tilde{N}$ for a system of density $\rho = 1$, in the liquid state, at temperatures $T = 1.2$ and 2.2. The steric shielding due to the presence of the first bonded neighbor at $\tilde{\theta} = 0°$ is captured by $\tilde{N}$ (bond 2−3 in Figure 1 is fixed in the $\tilde{x}_r$ system). In the screened region where $\tilde{N} = 0$, $\tilde{\bar{r}}$ is not defined. The steric shielding effect induces the peak in $\tilde{N}$ at angles $\tilde{\theta}$ close to $\pi/3$ and the significant increase in $\tilde{\bar{r}}$ in the vicinity of the screened region. The presence of the other bonded atom, at $\tilde{\theta} \approx \pi$ (bond 1−2 in Figure 1), does not visibly affect $\tilde{g}(\tilde{\mathbf{r}})$ since the bond can assume any position within a wide range of angles $\tilde{\theta}$. In fact, the upturn of $\tilde{N}$ at $\tilde{\theta} = \pi$ suggests that the shielding effect of the mobile bonded atom is weaker in that region and the probability distribution for the position of this bond in the intrinsic coordinate system has a maximum at about $\tilde{\theta} = 3\pi/4$. Similar conclusions can be drawn from Figure 3 which shows the dependence of $\tilde{N}$ upon density for systems of temperature $T = 1$. In denser systems and at low temperature, the peak at low $\tilde{\theta}$ increases in magnitude and becomes sharper about $\tilde{\theta} = \pi/3$. This position corresponds to the direction of maximum density in the solid state and the increase in magnitude of the peak suggests extensive close packed clustering of atoms in the system close to the glass transition.

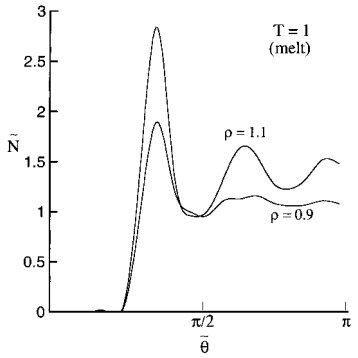

Figure 3. Dependence of the intrinsic atom number density distribution upon density, for systems in the liquid state.

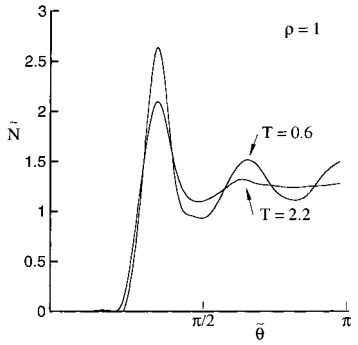

Figure 4. Effect of the glass transition on the intrinsic atom number density distribution. The system of density $\rho = 1$ is in the liquid state at $T = 2.2$ and in the glassy state at $T = 0.6$. The glass transition temperature for this system is $T_g = 0.85$. The peaks in the intrinsic distribution corresponding to the glassy state are centered about $\tilde{\theta}$, $2\pi/3$, and π, and indicate close packing. The behavior of the intrinsic atom number density distribution upon freezing is similar to that of the pair distribution function $g(r)$.

It is interesting to note the apparent similitude between the variation of $\tilde{N}$ with $\tilde{\theta}$, and that of the radial distribution function $g(r)$ with r. The steric shielding effect captured by $\tilde{N}(\tilde{\theta})$ at $\tilde{\theta} = 0°$ is not equivalent, however, with that evidenced by $g(r)$ at $r = 0$. While the effect seen in the radial distribution function is due to the representative atom to which the coordinate system is tied, and is similar in simple fluids and in systems of chains in equilibrium, in $\tilde{N}$ it is due to the first bonded neighbor of the same chain, and therefore the screening is absent in simple fluids. The parallel can be extended to the behavior of the two distributions during the glass transition. Figure 4 shows $\tilde{N}$ for a system of density $\rho = 1$ and at two temperatures, above ($T = 2.2$) and below ($T = 0.6$) the glass transition (for this system, $T_g \approx 0.85$). The evolution of structure is captured similarly by $\tilde{N}$ and $g(r)$ and hence, both measures can be used for the purpose of monitoring the transition. The sharp peaks that form in $\tilde{N}$ in the glassy state are centered about $\pi/3$, $2\pi/3$, and π and are due to close packing.

The distribution $\tilde{N}$ is computed from all nonbonded neighbors of a representative atom m, including neighbors belonging to other chains (interchain interactions) and atoms of the same chain which are not directly bonded to atom m (intrachain interactions), i.e., $\tilde{N} = \tilde{N}_{intra} + \tilde{N}_{inter}$. The shape of $\tilde{N}$ is similar for both inter- and intrachain contributions. In the short chain system ($N_b = 3$), $\tilde{N}_{intra} \ll \tilde{N}_{inter}$ at each $\tilde{\theta}$, due to topological constraints. The two contributions to $\tilde{N}$ have however similar magnitude in the long chain system ($N_b = 200$).

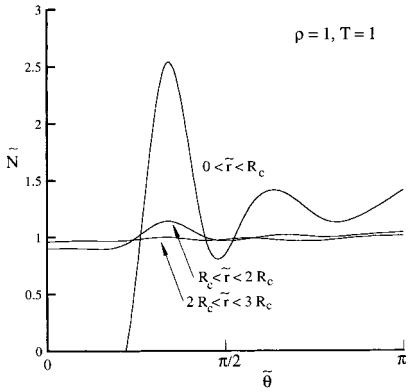

Figure 5. Intrinsic atom number density distribution for the system with $\rho = 1$ and $T = 1$, computed over 3 radial layers surrounding a representative atom (atom 2 in Figure 1). The steric shielding effect visible at low values of $\tilde{\theta}$ and for $\tilde{r} < R_c$, vanishes at distances $\tilde{r}$ from the representative atom larger than the covalent bond length b ($R_c = 2^{1/6}b$). This suggests that the intrinsic deviatoric stress is due to close range interactions only.

Let us turn now to the mechanism of stress production and the correlation between the intrinsic stress and intrinsic distribution. In a simple liquid in which the neighbor number density is constant about a representative atom, there is no deviatoric stress produced both locally and globally. It was shown[4] that, in order for nonhydrostatic stress to be produced in a simple liquid, the neighborhood of the representative atom has to be distorted. In systems of polymeric chains, however, such nonuniformity in the neighbors' distribution function is induced, in intrinsic coordinates, by the steric shielding effect. This, in turn, generates a nonzero deviatoric intrinsic stress even in absence of any deformation of the liquid. Further, in systems of polymeric chains, bonded interactions lead to an intrinsic stress tensor having only one nonzero component, $\tilde{\sigma}_{11}$[b]. In terms of parameters $\tilde{\tilde{r}}$ and $\tilde{N}$, the intrinsic nonbonded stresses are approximated by

$$\tilde{\sigma}_{ij} \approx \frac{3}{2R_c^3}\int_0^{\pi} \rho\tilde{N}(\sin\tilde{\theta})\tilde{\tilde{r}}u'(\tilde{\tilde{r}})\tilde{\tilde{r}}_i\tilde{\tilde{r}}_j\,d\tilde{\theta} \qquad (14)$$

The approximation is due to the fact that $\tilde{\tilde{r}}$ and $\tilde{N}$ represent the distribution function $\tilde{g}$ in a schematic manner only. The intrinsic deviatoric stress ${}^D\tilde{\sigma}_{ij}$ can be computed from eq 14 as

$${}^D\tilde{\sigma}_{11} = \tilde{\sigma}_{11} - \frac{1}{3}\tilde{\sigma}_{kk} = \frac{1}{R_c^3}\int_0^{\pi} \rho\tilde{N}(\sin\tilde{\theta})\tilde{\tilde{r}}u'(\tilde{\tilde{r}})\tilde{P}_2(\tilde{\theta})\,d\tilde{\theta} \qquad (15)$$

where $\tilde{P}_2(\tilde{\theta}) = {}^1/_2(3\cos^2\tilde{\theta} - 1)$ is the second Legendre polynomial. The existence of a nonzero deviatoric stress in intrinsic coordinates, in equilibrium, is relevant for the mechanism of global stress production in nonequilibrium. This issue will be discussed in the following subsection.

Further insight into the mechanism of intrinsic stress production can be gained by analyzing the distribution $\tilde{N}$ at larger distances from the representative atom. For this purpose, $\tilde{N}$ was computed for the system with ($\rho = 1$, $T = 1$), over radial layers with $0 < \tilde{r} < R_c$, $R_c < \tilde{r} < 2R_c$ and $2R_c < \tilde{r} < 3R_c$, with $R_c = 2^{1/6}\sigma_{LJ}$. Figure 5 shows the variation of $\tilde{N}$ with $\tilde{\theta}$ for the three regions. As the distance from the representative atom increases, the

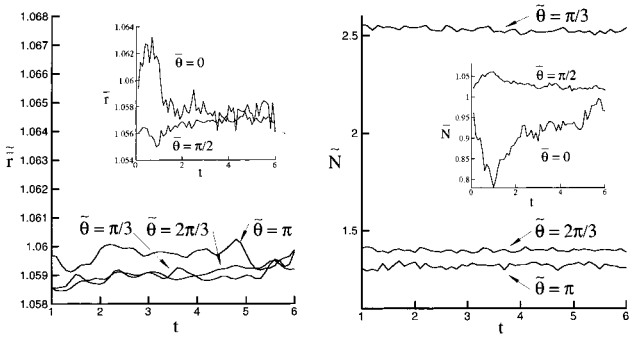

Figure 6. Time variation of the intrinsic distribution during stress relaxation for the system with $\rho = 1$ and $T = 1$. Time $t = 1$ represents the end of the loading period and beginning of a relaxation regime in which the simulation cell size and shape remain unchanged. The two parameters $\tilde{\bar{r}}$ and $\tilde{N}$ characterizing the intrinsic distribution function $\tilde{g}$ are shown for three sectors of angular span 10° centered at $\tilde{\theta} = \pi/3$, $2\pi/3$, and π. The intrinsic distribution is seen to be independent of the deformation of the fluid during relaxation. The insets show the variation of the equivalent parameters $\bar{r}$ and $\bar{N}$ that characterize the pair distribution function $g(r)$ in global coordinates. Both loading and relaxation periods are shown in the insets (loading begins at $t = 0$ and ends at $t = 1$), while the intrinsic distribution is represented during relaxation only ($t > 1$). The fast relaxation of $\bar{r}$ for $1 \leq t < 4$ corresponds to the first global stress relaxation mode. $\bar{N}$ relaxes at a slower rate due to its dependence upon bond orientation. The figure shows that the intrinsic distribution sets a structural invariant to deformation.

distribution of neighbors becomes uniform in the $\tilde{\theta}$ direction since the influence of the steric shielding effect diminishes. This indicates that the deviatoric intrinsic stress is produced essentially by neighbors within a distance from the representative atom smaller than the bond length and is due to the excluded volume effect. Since this argument is based on geometric considerations, it is expected to remain valid in systems with larger cutoff distance R_c.

Nonequilibrium Simulations. Nonequilibrium simulations have been performed on short chain and long chain systems in order to identify the structural changes that accompany stress relaxation. Figure 6 shows the variation of $\tilde{\bar{r}}$ and $\tilde{N}$ during stress relaxation in a short chain system of $\rho = 1$ and $T = 1$. Time $t = 1$ corresponds to the end of the loading period. For $t > 1$, the size and shape of the simulation cell are kept constant and the system relaxes to isotropy. The time variation of the two parameters is shown for 3 angular sectors, each spanning 10° and centered at $\tilde{\theta} = \pi/3$, $2\pi/3$, and π. Both measures of the intrinsic distribution function are deformation independent. Thus, $\tilde{\bar{r}}$ and $\tilde{N}$ define a structural invariant to deformation.

For comparison, the variation of the equivalent measures of structure, $\bar{r}$ and $\bar{N}$,[4,5] characterizing $g(\mathbf{r})$ in the global coordinate system, are shown in the inset of Figure 6, for $\bar{\theta} = 0$ and $\pi/2$. $\bar{\theta} = 0$ is parallel to x_1, the stretch direction of the simulation cell. During deformation, the number density in the forward direction ($\bar{\theta} = 0$) drops sharply, with the reversed trend being observed for $\bar{\theta} = \pi/2$. $\bar{r}$ captures an equivalent effect. Apart from the striking difference between the sensitivity to deformation of $\bar{r}$ and $\bar{N}$, and the insensitivity of the equivalent intrinsic measures $\tilde{\bar{r}}$ and $\tilde{N}$, it is interesting to note the difference in the relaxation behavior of $\bar{r}$ and $\bar{N}$. While $\bar{r}$ undergoes a fast return to isotropy through a nonexponential mode,[4] $\bar{N}$ isotropization is much slower.

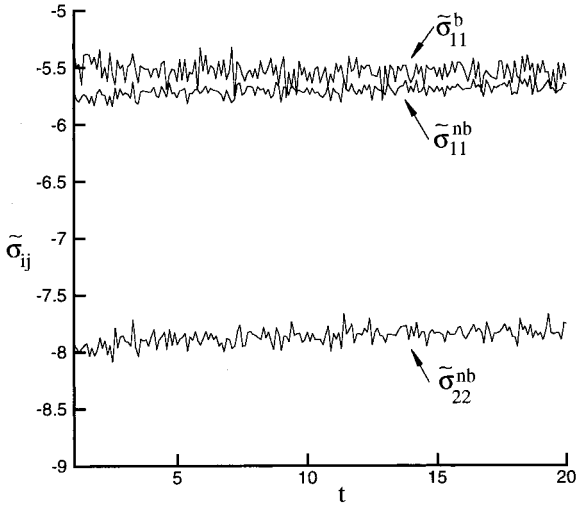

Figure 7. Intrinsic stresses computed during the relaxation period of the system shown in Figure 6. As suggested by the deformation independence of the intrinsic distribution, the intrinsic stresses are also insensitive to deformation. Intrinsic stresses due to both bonded σ_{11}^{b} and nonbonded σ_{11}^{nb} interactions are shown, with the nonbonded stress being due to intra- and interchain interactions. Both components are cylindrical tensors, with the only nonzero terms being those shown. Note that $\sigma_{22}^{nb} = \sigma_{33}^{nb}$.

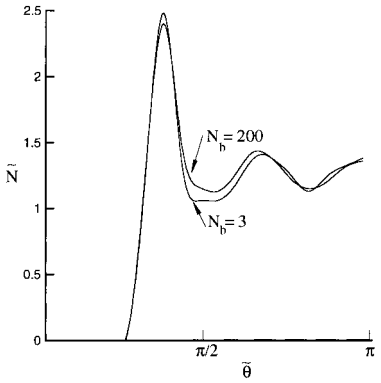

Figure 8. Intrinsic atom number density distribution for systems of different chain lengths and $\rho = 1$ and $T = 1$. When computed from chain inner atoms, the intrinsic distribution is chain length independent.

The invariance of $\tilde{g}$ to deformation implies that the intrinsic stresses are also deformation insensitive, eqs 14 and 15. Figure 7 shows the nonzero components of the intrinsic stress tensor $\langle\langle\tilde{\sigma}_{ij}\rangle\rangle$ for the whole relaxation history of the same system. Both bonded and nonbonded intrinsic stresses are shown, with the nonbonded component including the effect of both inter- and intrachain interactions.

The mechanism of stress production is seen to be identical in short chain and long chain systems. Figure 8 shows $\tilde{N}$ computed from the $N_b = 3$ and $N_b = 200$ systems of same density and temperature ($\rho = 1$, $T = 1$) and subjected to the same deformation program. The distribution has been computed from chain inner atoms only. Since $\tilde{g}$ is independent of deformation in both systems, the relaxation time at which these data have been collected is not important. When computed from chain inner atoms, the intrinsic distribution is seen to be essentially chain length independent. The atoms located at chain ends have, in intrinsic coordinates, a distribution of neighbors which resembles that found in a diatomic liquid of the same density and tempera-

ture. This finding substantiates the observed invariance of the intrinsic stresses with the chain length.[15]

In light of these findings, it is useful to identify the framework in which the relationship between stress relaxation and structural changes is best described. To this end, it is necessary to put the present data in relation with the conclusions of previous work.[11,14,15]

Stress relaxation has two regimes. The first regime is a fast nonexponential mode which accounts for the relaxation of the largest part of stress. The stress produced during loading has both an energetic and an entropic character. The energetic stress is due to the loss of isotropy of the neighborhood of a representative atom[4] and to stretch effects, while the entropic component is due to the preferential orientation of bonds (intrinsic frames) during deformation.[5] The first relaxation mode corresponds primarily to the relaxation of the energetic component. Hence, the structural changes observed during this period consist in the return to isotropy of the neighborhood of a representative atom and are captured by $\bar{r}$[4] (inset of Figure 6). $\tilde{\bar{r}}$ however is seen here to be weakly sensitive to such structural changes. The insensitiveness of $\tilde{\bar{r}}$ to deformation is due to the fact that the intrinsic coordinate system $\tilde{x}_i$ (or bond orientation) equally samples all possible spatial orientations. This invariance is expected to break down at high degrees of bond orientation. Such extreme alignment, however, is not likely to occur in melts at high temperatures and during deformation of reasonable strain rates.

During the second relaxation mode the global stress is proportional to $P_2{}^b$. Here $P_2{}^b = \langle\langle {}^1/_2(3\cos^2\theta_b - 1)\rangle\rangle$ is a measure of average bond orientation with respect to the global coordinate system, and θ_b is the angle made by a bond with the x_1 axis. In this regime, stress has an entropic character and is proportional to birefringence through the stress−optical coefficient, $\tau = \tau_b + \tau_{nb} = CP_2{}^b$ (τ is the global stress difference $\tau = t_{11} - {}^1/_2(t_{22} + t_{33})$, with t_{ij} given by eq 10, and τ_b and τ_{nb} are the bonded and nonbonded contributions, respectively). Further, the stress−optical coefficient SOC $=1/C$, with C being expressed in terms of intrinsic deviatoric stresses as $C = 3/2\rho[\langle\langle {}^D\tilde{\sigma}_{11}{}^b\rangle\rangle + D\langle\langle {}^D\tilde{\sigma}_{11}{}^{nb}\rangle\rangle]$.[5,15] In this regime, the relationship between stress production and relaxation on the one hand and structural changes on the other is readily captured in intrinsic coordinates. The deformation insensitiveness of the intrinsic distribution leads to time independent intrinsic stresses and hence to a constant stress−optical coefficient. The global deviatoric stress is then due to the preferential orientation of bonds induced by deformation, with each bond carrying a nonzero, deformation insensitive intrinsic deviatoric stress. A random orientation of bonds, in equilibrium, induces a hydrostatic global stress only.

Hence, it appears that the relationship between structural changes and global stress during the first fast relaxation mode is best described in the global frame ($\bar{r}$), while the intrinsic frame ($\tilde{\bar{r}}$ and $\tilde{N}$) is better suited for this representation at later times, during the second relaxation mode.

5. Conclusions

The mechanisms of stress production and relaxation in model polymeric systems of short and long molecules have been identified, and the relationship between stress and the distribution of interacting atoms about a representative atom has been established. The analysis of the variation of the intrinsic distribution with temperature and density demonstrated its effectiveness in capturing packing effects and in monitoring the glass transition. The nonuniformity of the intrinsic distribution induces an intrinsic deviatoric stress in systems in both equilibrium and nonequilibrium. Only close range interactions are observed to contribute to the intrinsic deviatoric stress production. In nonequilibrium, it was shown that, during a constant volume elongational deformation of the melt, the distribution of interacting atoms expressed in intrinsic coordinates is deformation and chain length independent. This conclusion is expected to also hold true for other types of melt deformation. These observations substantiate the proportionality between macroscopic stress and birefringence observed over a wide regime at elevated temperatures and when stretching effects are not dominant. They further show that the mechanism of stress production is independent of chain length.

Acknowledgment. The author thanks Prof. J. H. Weiner for encouragement and many fruitful discussions.

References and Notes

(1) Heyes, D. M. *J. Phys. Cond. Matter* **1994**, *6*, 6409−6419.
(2) Heyes, D. M.; Kim, J. J.; Montrose, C. J.; Litovitz, T. A. *J. Chem. Phys.* **1980**, *73*, 3987−3995.
(3) Heyes, D. M.; Montrose, C. J.; Litovitz, T. A. *J. Chem. Soc., Faraday Trans.* **1983**, *79*, 611−635.
(4) Picu, R. C.; Weiner, J. H. *J. Chem. Phys.* **1997**, *107*, 7214−7222.
(5) Picu, R. C.; Weiner, J. H. *J. Chem. Phys.* **1998**, *108*, 4984−4991.
(6) Rouse, P. E. *J. Chem. Phys.* **1953**, *21*, 1272−1285.
(7) Doi, M.; Edwards, S. F. *The theory of polymer dynamics*; Clarendon: Oxford, England, 1986.
(8) Bird, R. B.; Curtis, C. F.; Armstrong, R. C.; Hassager, O. *Dynamics of polymeric liquids: Kinetic theory*; Wiley-Interscience: New York, 1987.
(9) Kanaya, T.; Kawaguchi, T.; Kaji, K. *J. Chem. Phys.* **1996**, *104*, 3841−3850.
(10) Roe, R. J. *J. Non-Cryst. Solids* **1998**, *235−237*, 308−313.
(11) Gao, J.; Weiner, J. H. *Macromolecules* **1996**, *29*, 6048−6055.
(12) Gao, J.; Weiner, J. H. *Macromolecules* **1992**, *25*, 3462−3467.
(13) Kroger, M.; Luap, C.; Muller, R. *Macromolecules* **1997**, *30*, 526−539.
(14) Loriot, G.; Weiner, J. H. *J. Polym. Sci: Polym. Phys.* **1998**, *36*, 143−154.
(15) Picu, R. C.; Loriot, G.; Weiner, J. H. *J. Chem. Phys.* **1999**, *110*, 4678−4686.
(16) Gao, J.; Weiner, J. H. *J. Chem. Phys.* **1989**, *90*, 6749−6760.
(17) Berendsen, H.; Postma, J.; van Gunsteren, W. *J. Chem. Phys.* **1984**, *81*, 3684−3693.
(18) Swenson, R. W. *Am. J. Phys.* **1987**, *55*, 746−751.

MA990836Q